American Mineralogist, Volume 84, pages 607–619, 1999

The smectite to chlorite transition in the Chipilapa geothermal system, El Salvador

D. ROBINSON[1,*] AND A. SANTANA DE ZAMORA[2]

[1]Department of Earth Sciences, Wills Building, Queens Road, University of Bristol, BS8 1RJ, U.K.
[2]Comision Ejecutiva Hidroelectrica del Rio Lempa, El Salvador

ABSTRACT

Clay mineralogical X-ray diffraction and electron microprobe studies have been carried out on separated <2 μm fractions from cutting and core material from three wells in the Chipilapa geothermal system in El Salvador. The data indicate that the smectite to chlorite transition is prevalent, but a secondary smectite to illite transition is also present. At depths approximately <750 m, smectite with very minor chlorite mixed-layers (approximately <15%) is dominant, and has a composition midway between a di- and tri-smectite. At ~750 m there is a very clear distinction and sharp transition into discrete chlorite with very minor smectite mixed-layers (approximately <10%). Corrensite is recorded only as a rare and minor phase.

Smectite occurs in abundance at temperatures up to ~200 °C, and the transition from a smectite-dominant to chlorite-dominant assemblage takes place over a narrow temperature range (~150 to 200 °C). The stability range of smectite is very similar to that recorded in other geothermal systems, whereas the smectite to chlorite transition differs greatly from that recorded in other systems. The transition does not involve continuous chlorite/smectite mixed-layering but a marked step: It is the sharpest and most discontinuous stepped sequence of this mineralogical transition recorded.

INTRODUCTION

Mineralogic reactions in clay minerals, particularly the low-temperature conversion of dioctahedral smectite to illite and trioctahedral smectite to chlorite, have attracted much interest in recent years. The latter series is perhaps the most ubiquitous of all mineralogical reactions in basic-intermediate rocks of the shallow crust, but there are many critical points about the transition that are the subject of on-going debate. These include features such as the actual mineralogic nature of the reaction, and its application as a geothermometer and as an indicator of fluid-rock interaction.

The traditional model for the tri-smectite to chlorite reaction is that of a continuous sequence of chlorite/smectite mixed-layering between the two end-members, with increasing temperature giving rise to an increased percentage of chlorite layers. Well-documented examples of mixed-layer chlorite/smectite have been reported from regional and geothermal settings (e.g., Bettison-Varga et al. 1991; Schiffman and Fridleifsson 1991; Robinson et al. 1993; Robinson and Bevins 1994). More recently, an alternative model has been proposed that involves a discontinuous change from smectite to corrensite to chlorite without chlorite/smectite mixed-layering, and examples have been reported from sea mount, sea floor, and regional settings (e.g., Shau et al. 1990; Schiffman and Staudigel 1995; Schmidt and Robinson 1997). In this model, corrensite is regarded as a discrete phase and not as a 50:50 mixed-layer chlorite/smectite phase (Reynolds 1988; Shau et al. 1990). To account for these two different reported reaction styles, it has been proposed that the discontinuous transition represents an equilibrium sequence favored in situations where fluid/rock ratios are high. By contrast, the continuous mixed-layer series may represent a metastable progression associated with incomplete reaction and/or low integrated fluid/rock ratios (Schiffman and Staudigel 1995; Schiffman 1995). An example where different mafic phyllosilicate assemblages have developed in response to postulated differences in fluid/rock ratios is from Kewennawan basaltic flows metamorphosed under subgreenschist facies conditions. Smectite is dominant in the massive parts of flow centers, whereas within <10 m in highly amygdaloidal flow tops, corrensite and/or chlorite dominate (Schmidt and Robinson 1997).

The smectite-to-chlorite transition has been applied widely as a qualitative measure of metamorphic grade. This has been carried out by documenting the increasing proportions of chlorite layers, or by correlating the progressive changes in the smectite to chlorite transition to well temperatures in modern geothermal systems (e.g., Kristmannsdóttir 1979; Schiffman and Fridleifsson 1993). In addition, the substitution of Si by Al in the tetrahedral position of chlorite also has been applied widely as a geothermometer (Cathelineau 1988).

There is also debate about the extent to which the above type of clay-mineral reactions, as well as the clay-mineral assemblages themselves, might develop progressively in response to equilibrium stability, or whether they represent non-equilibrium conditions and are controlled more by kinetic effects (Essene and Peacor 1995). These considerations have important implications as to whether interpretation of clay mineral

*E-mail: Doug.Robinson@bristol.ac.uk

parameters of a general (e.g., illite crystallinity, mixed-layer progression) or more specific character [^{IV}Al in chlorite thermometer (Cathelineau 1988; Bevins et al. 1991)] can provide precise temperature estimates or only very broad estimates of grade (Essene and Peacor 1995).

In this study we characterize the mafic phyllosilicate assemblages in the Chipilapa, El Salvador geothermal system, including the nature of the mineralogic transition, and its relation to well temperatures and chemical characters, as a means of addressing some of the above concerns. The effects of fluid-rock interaction in the Chipilapa geothermal field have been investigated recently through fluid inclusion study and by analysis of the <2 μm and <0.2 μm clay fractions (Beaufort et al. 1995; Bril et al. 1996; Patrier et al. 1996). Although these studies provided data on the distribution of the illite/smectite and chlorite/smectite series in the geothermal system, the clay-mineral assemblages were interpreted in relation to the overall evolution of the field and a general comparison between their development in geothermal and in diagenetic pelitic systems. Although the data were of direct relevance to many of the points of on-going debate and controversy with respect to the smectite to chlorite reaction, none of the items outlined above were considered. Indeed, the smectite to chlorite reaction style recorded for the Chipilapa system contrasts to previously reported examples, so that verification of its unique style is a further important aim of this study.

GEOLOGIC SETTING

The geology of El Salvador is dominated by a west-northwest–east-southeast trending Pleistocene volcanic arc system formed as a result of northeastward subduction of the Cocos plate under the Caribbean plate. A series of volcanic edifices reaching up to 1900 m were formed in this system and are of Pleistocene to Holocene age. A major topographic feature associated with the volcanic system is an east-trending Central Graben formed during the Quaternary. Various geothermal systems are developed along the intersection of the southern boundary fault of the Central Graben with the inner slope of the young volcanic chain. These geothermal systems show surface expressions in the form of hot springs, fumaroles, and steaming ground. Five major geothermal fields have been developed in the graben (Fig. 1) and the samples examined in this study are from the Ahuachapan-Chipilapa field, which lies to the west of the graben.

THE AHUACHAPAN-CHIPILAPA GEOTHERMAL SYSTEM

This field is developed within a caldera structure whose complex patterns of faults, superimposed on the graben, provide the channelways for the geothermal systems and fumaroles. The major east-west/northeast-southwest graben boundary faults are older and more-major than a set of north-south trending, more-minor transverse faults, but are younger and probably still active. The geothermal fluids of the reservoir zone of this field are believed to be derived from fluids of meteoric origin present at depth beneath the Recent volcanic rocks to the south. These fluids are thought to use the graben-bounding faults as the main conduits for northward movement, which are then channelled into the transverse faults for their final rise to the surface (Aumento et al. 1982; Bril et al. 1996).

A preliminary stratigraphy has been established for the

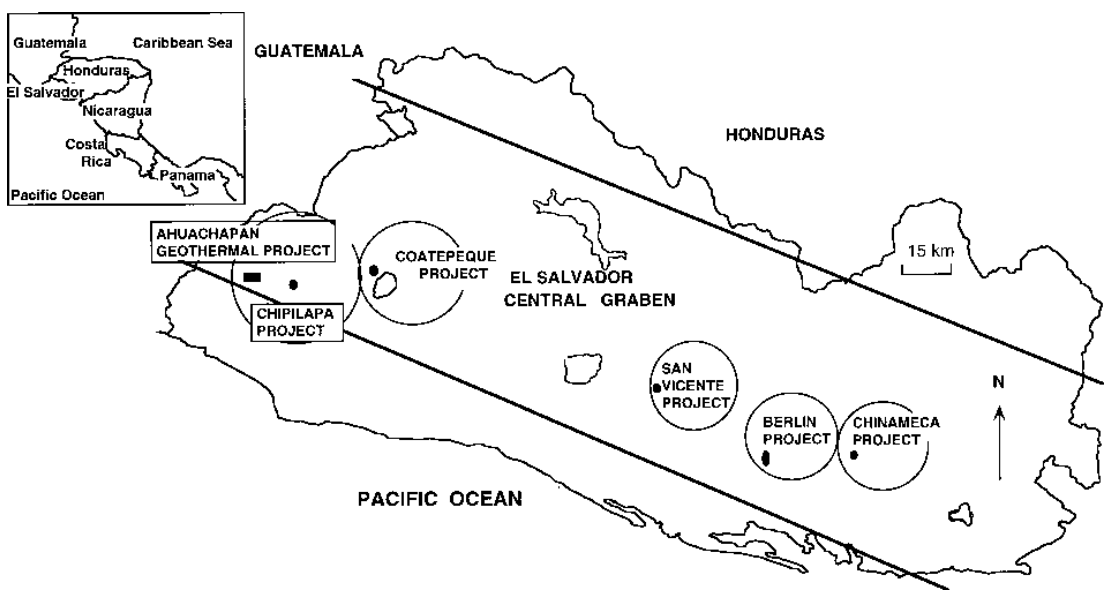

FIGURE 1. Map of El Salvador showing location of geothermal projects within the central graben. The Chipilapa system is located at the very western end of the country. The inset map shows the location of El Salvador within Central America.

nearby Ahuachapan field in which there is an ~200 m cover of Holocene age, followed by ~800 m of interbedded lavas and volcaniclastic horizons below which lava sequences dominate. Overall, the volcanic sequence ranges from basaltic andesites to dacites, with the predominant lava type being andesite (Cuellar et al. 1981; Aumento et al. 1982). Detailed mineralogic study of 1000 samples taken from 31 wells drilled within a 6 km^2 region of this field (Aumento et al. 1982) revealed extensive recrystallization with secondary minerals commonly in excess of 50% of the samples and locally up to 90%. In addition, recent studies of the fluid inclusions and clay mineralogy (Beaufort et al. 1995; Bril et al. 1996; Patrier et al. 1996) have been used to suggest that the field developed in a three-stage history involving (1) initiation of a conductive thermal gradient with propylitic alteration; (2) influx of meteoric water along fractures and crystallization of mixed-layer clays; and (3) restoration of the conductive thermal gradient and conversion of mixed-layer clays to illite and chlorite. The present-day stage is represented by active fluid circulation along faults and precipitation of smectite.

Three wells (CH7, CH8, and CH9) from the Chipilapa field that are ~1 km apart have been examined using both core and cutting material, although core material is largely restricted to deeper parts of the wells where spot coring was performed at restricted and irregular intervals. Well CH7 reached a maximum depth of 1501 m, where a temperature of 195 °C was recorded (Fig. 2). This well has two regions where very rapid increases in temperature occur between ~250–500 m and from ~1250 m to the base at 1500 m. These two regions have been equated with postulated reservoir zones (cf. Fig. 2 of Bril et al. 1996). Well CH8 reaches a depth of 2556 m at a temperature of 228 °C. The overall downwell temperature pattern is similar to that of CH7 with a step in the thermal profile at ~500 m, although no reservoir zone is postulated at this approximate depth for this borehole. Below ~500 m there is a rapid rise in temperature to ~170 °C followed by a flatter profile to ~1500 m, before temperature again starts to rise steeply (Fig. 2). Well CH9 is the deepest one, reaching 2001 m where a temperature of 223 °C was recorded. The overall thermal profile for CH9 is less sharply stepped than for CH7 and CH8, although the effect of the thermal anomaly at ~500 m is still evident. Here, there is a steep rise in temperature from ~100 to 150 °C marking the position of the shallowest reservoir, after which the profile is more continuous marking its position a small distance to the northwest of the thermal anomaly (cf. Fig. 2 of Bril et al. 1996).

Although the general volcaniclastic and lava sequences encountered in the three wells range in composition from basaltic andesite to dacite (Aumento et al. 1982; Cuellar et al. 1981), the lithologic types in each well are not well known. This arises because core material was taken only at restricted and irregular intervals with dominantly only cutting material available, and that material commonly is extensively and pervasively altered, making definitive recognition of protolith type difficult. Using available petrographic data, and previous information from Aumento et al. (1982), Cuellar et al. (1981), Patrier et al. (1996), and Santana de Zamora (1991), the broadly known lithologic types for each of the wells are given as simplified lithologic logs in Figures 3, 4, and 5.

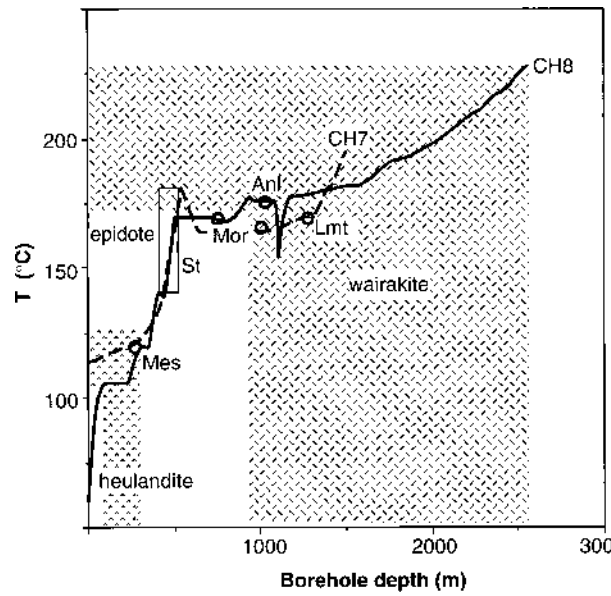

FIGURE 2. Well temperature vs. well depth diagram showing the thermal profiles in CH7 and CH8 for which zeolite and calc-silicate occurrence data are available. The extent of heulandite, epidote, and wairakite distributions are shown by the ornamented areas. The epidote field shown also extends over the whole field outlined for wairakite. Mes = mesolite, St = stilbite, Mor = mordenite, Anl = analcime, and Lmt = laumontite.

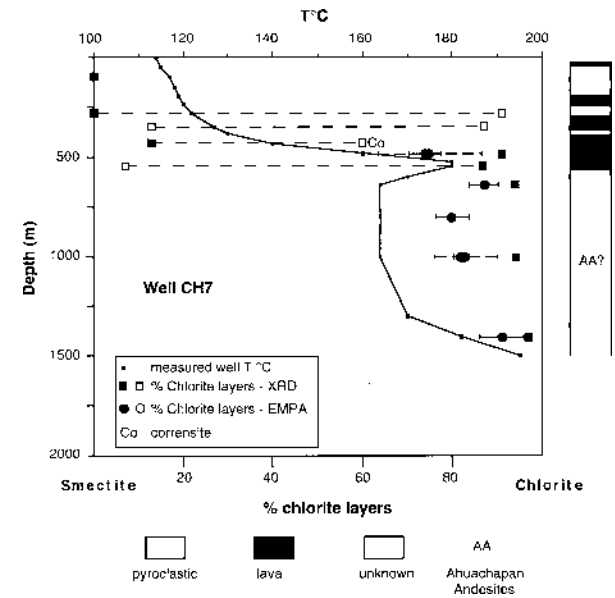

FIGURE 3. Distribution of mafic phyllosilicate minerals as determined by XRD (square symbols) and EMPA (circle symbols) in well CH7 plotted against depth (*y* axis), temperature (*x* axis, upper scale), and percentage of chlorite layers (*x* axis, lower scale). Solid and open symbols represent, respectively, major and minor occurrences of phase. Depth-temperature profile for well shown as solid line. Error bars (1σ) shown for repeat analyses by EMP. Broad lithologic types in well shown in column, based on petrographic data and information from Aumento et al. (1982), Cuellar et al. (1981), Patrier et al. (1996), and Santana de Zamora (1991).

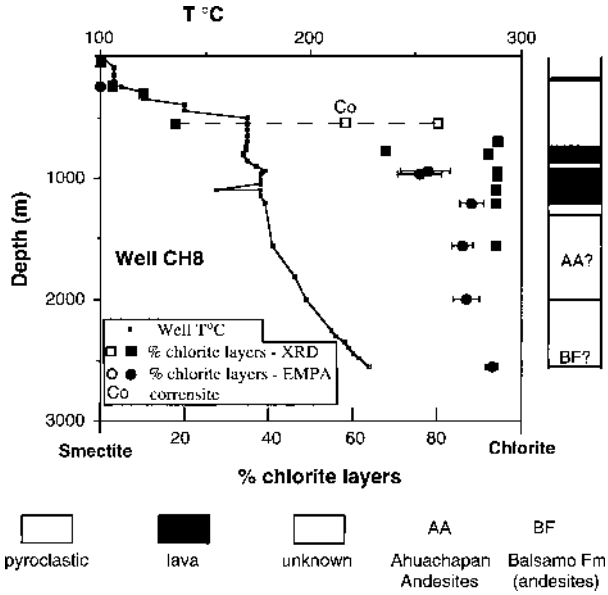

FIGURE 4. Distribution of mafic phyllosilicate minerals in well CH8 plotted against depth (*y* axis), temperature (*x* axis, upper scale), and percentage chlorite layers (*x* axis, lower scale). Other symbols and data as Figure 3.

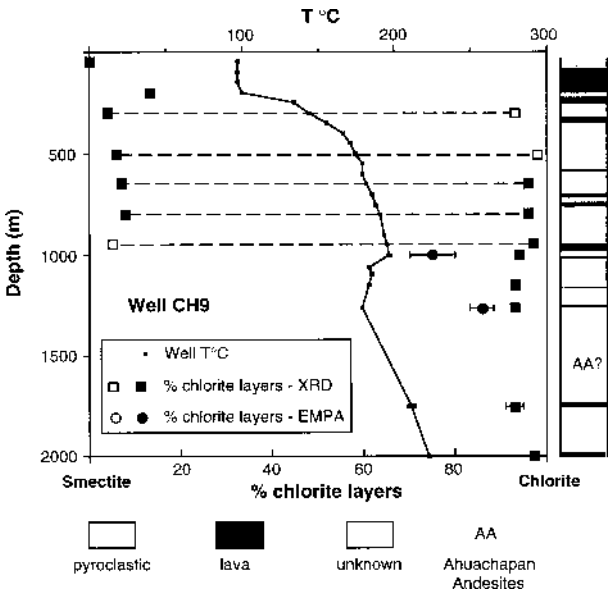

FIGURE 5. Distribution of mafic phyllosilicate minerals in well CH9 plotted against depth (*y* axis), temperature (*x* axis, upper scale), and percentage chlorite layers (*x* axis, lower scale). Other symbols and data as Figure 3.

ANALYTICAL PROCEDURE

The <2 μm clay fractions were prepared for X-ray diffraction (XRD) by ultrasonic treatment of small rock chips to separate the phyllosilicate material from the rock matrix. This material was collected by centrifuge and vacuum filtration through 0.45 μm millipore filters and then spread evenly onto a glass plate by pipetting. Glycol solvation was carried out at 60 °C for a minimum of two days. A Philips PW1800 diffractometer was used, with Cu*K*α radiation (at 40 kV and 50 mA), automatic divergence slit, fine receiving slit, and graphite monochromator. Count data were collected at intervals of 0.02° 2θ for a time of 2 s. Most XRD samples examined were dominated by mafic phyllosilicates with subordinate illitic clays. The proportions of mixed-layers in the chloritic and illitic material were determined by measurement of the 002 peak migration curves of Reynolds (1980, 1988). The type of mixed layer was identified from the position of the 002 peak, an 8.52 Å position being indicative of a pure smectite whereas migration to higher or lower *d* values indicate illite/smectite or chlorite/smectite, respectively. Electron microprobe (EMP) analysis of mafic phyllosilicates was carried out using a JEOL JXA 8600 superprobe. Average compositions of the mafic phyllosilicates in the three wells are given in Table 1. Percentages of the chlorite layers (x) were calculated using the method of Wise [quoted in Bettison and Schiffman (1988)] and are given in Table 1 along with the temperature derived from the Cathelineau (1988) thermometer.

RESULTS

Secondary recrystallization and mineralogy

Preliminary documentation of the extent of secondary recrystallization and the types of minerals present, including zeolites and calc-silicate minerals, is available for wells CH7 and CH8 (Santana de Zamora 1991). The secondary mineralogy typically forms some 40–55% of the rocks indicating pervasive and extensive recrystallization of the protoliths. Phyllosilicates are the main secondary phases, which reach up to some 30–40%, with mafic phyllosilicates predominant in their occurrence and abundance. Quartz and calcite are ubiquitous throughout the sequences, reaching up to ~20 and ~10%, respectively. Zeolites typically total to <10%, with heulandite being the dominant zeolite at depths <300 m and over a narrow temperature range of 106–122 °C, followed in a downhole progression over the temperature range 120–170 °C by mesolite, stilbite, mordenite, analcime, and laumontite (Fig. 2). From ~170 °C to the maximum temperature of 228 °C at the base of CH8, wairakite is the only zeolite present. Epidote is also common at temperatures above 164 °C, below depths of ~1000 m.

Mafic phyllosilicates

Well CH7. Mafic phyllosilicates were characterized by XRD and EMP analysis of 12 samples and are shown in Figure 3. Below 484m, XRD and EMP data are from cored samples, whereas at shallower depths, only XRD data from cuttings are available. XRD patterns of two samples from 100 m (117 °C) and 284 m (122 °C) are dominated by smectite with strong 001 peaks at ~17 Å and five higher-order, but weaker peaks; in both cases peak positions indicate pure smectite with no chlorite mixed layering. In the sample from 284 m, small peaks at 7.19 (002) and 3.58 Å (004) indicate minor amounts of chlorite.

At greater depths, between ~350 and 550 m (127–180 °C), XRD patterns of four samples (CH7-8, CH7-10, CH7-13, and CH7-15) show two distinct phyllosilicates in three of the four samples (Fig. 3, Table 2a). In CH7-8, from 350 m, a nearly

TABLE 1a. EMP analyses of mafic phyllosilicates from cored samples from well CH7

sample	484 (12)	sd	486 (15)	sd	641 (17)	sd	803 (10)	sd	1001 (24)	sd	1003 (4)	sd	1404 (7)	sd
SiO_2	28.85	1.19	29.63	1.07	27.39	0.97	29.47	0.62	26.57	1.49	27.32	0.81	25.56	0.91
TiO_2	0.01	0.03	0.02	0.04	0.03	0.04	0.02	0.03	0.06	0.06	0.00	0.00	0.04	0.06
Al_2O_3	18.22	0.74	17.82	0.85	18.30	0.55	19.21	0.20	19.20	0.92	19.27	0.72	20.21	0.96
FeO_T	22.28	0.65	21.01	0.82	28.13	1.18	20.87	2.94	27.06	2.04	24.22	1.94	26.34	2.53
MnO	0.36	0.06	0.42	0.05	0.32	0.06	0.89	0.11	0.70	0.12	0.66	0.10	0.75	0.08
MgO	15.78	1.66	16.98	0.89	13.20	0.76	18.41	2.20	12.74	2.21	14.62	1.79	13.20	1.80
CaO	0.41	0.08	0.42	0.12	0.20	0.04	0.24	0.05	0.27	0.12	0.27	0.06	0.13	0.05
Na_2O	0.05	0.02	0.12	0.03	0.04	0.02	0.03	0.01	0.09	0.06	0.10	0.01	0.09	0.08
K_2O	0.12	0.07	0.09	0.05	0.03	0.02	0.07	0.05	0.13	0.14	0.09	0.06	0.04	0.04
Total	86.09		86.51		87.65		89.20		86.84		86.54		86.38	
Formulae based on 28 O atoms														
Si	6.07	0.19	6.16	0.11	5.86	0.06	5.94	0.04	5.73	0.20	5.81	0.11	5.53	0.15
Ti	0.00	0.00	0.00	0.01	0.00	0.01	0.00	0.01	0.01	0.01	0.00	0.00	0.01	0.01
^{IV}Al	1.93	0.19	1.84	0.11	2.14	0.06	2.06	0.04	2.27	0.20	2.19	0.11	2.47	0.15
^{IV}Al	2.60	0.28	2.53	0.14	2.47	0.07	2.51	0.04	2.61	0.19	2.63	0.08	2.68	0.14
Fe	3.92	0.11	3.65	0.17	5.03	0.26	3.52	0.55	4.88	0.45	4.31	0.42	4.76	0.51
Mn	0.06	0.01	0.07	0.01	0.06	0.01	0.15	0.02	0.13	0.02	0.12	0.02	0.14	0.01
Mg	4.95	0.48	5.26	0.15	4.21	0.18	5.53	0.59	4.09	0.64	4.63	0.48	4.25	0.51
NIC	19.54	0.22	19.52	0.07	19.77	0.06	19.71	0.02	19.71	0.13	19.69	0.03	19.83	0.08
Ca	0.09	0.02	0.09	0.03	0.05	0.01	0.05	0.01	0.06	0.03	0.06	0.01	0.03	0.01
Na	0.02	0.01	0.05	0.01	0.02	0.01	0.01	0.01	0.04	0.03	0.04	0.00	0.04	0.03
K	0.03	0.02	0.02	0.01	0.01	0.00	0.02	0.01	0.04	0.04	0.03	0.02	0.01	0.01
IC	0.15	0.03	0.17	0.03	0.07	0.01	0.08	0.02	0.14	0.04	0.13	0.01	0.08	0.05
XMg	0.56	0.03	0.59	0.02	0.46	0.02	0.61	0.06	0.46	0.06	0.52	0.05	0.47	0.06
x	0.75	0.12	0.74	0.04	0.87	0.03	0.84	0.01	0.84	0.07	0.82	0.02	0.91	0.05
Formulae based on variable number of O atoms as indicated														
Ox	26.5		26.4		27.2		27.0		27.1		26.9		27.4	
Si	5.75	0.18	5.81	0.10	5.70	0.06	5.88	0.04	5.54	0.19	5.59	0.11	5.42	0.14
^{IV}Al	2.25	0.18	2.19	0.10	2.30	0.06	2.12	0.04	2.46	0.19	2.41	0.11	2.58	0.14
Ti	0.00	0.00	0.00	0.01	0.00	0.01	0.00	0.00	0.01	0.01	0.00	0.00	0.01	0.01
^{VI}Al	2.02	0.28	1.94	0.14	2.18	0.07	2.39	0.04	2.25	0.19	2.23	0.08	2.46	0.14
Fe	3.71	0.11	3.45	0.17	4.89	0.25	3.48	0.55	4.72	0.44	4.14	0.42	4.67	0.50
Mn	0.06	0.01	0.07	0.01	0.06	0.01	0.15	0.02	0.12	0.02	0.11	0.02	0.13	0.01
Mg	4.68	0.48	4.97	0.15	4.09	0.18	5.47	0.58	3.96	0.63	4.46	0.47	4.17	0.50
NIC	18.48	0.22	18.42	0.07	19.22	0.06	19.50	0.02	19.06	0.13	18.95	0.03	19.44	0.09
Ca	0.09	0.02	0.09	0.02	0.05	0.01	0.05	0.01	0.06	0.03	0.06	0.01	0.03	0.01
Na	0.02	0.01	0.05	0.01	0.02	0.01	0.01	0.01	0.04	0.03	0.04	0.00	0.04	0.03
K	0.03	0.02	0.02	0.01	0.01	0.00	0.02	0.01	0.03	0.04	0.02	0.02	0.01	0.01
IC	0.14	0.03	0.16	0.03	0.07	0.01	0.08	0.02	0.13	0.04	0.12	0.01	0.08	0.0
T °C	301	30	290	17	309	9	280	7	335	31	326	17	354	23

Notes: Figure under sample heading is depth (m) of sample in well, and number of repeat analyses given in parentheses for which standard deviation (sd) is calculated. x value is percentage of chlorite layers, and *T* °C is temperature derived from chlorite thermometer. FeO_T total iron as FeO.

pure chlorite with 13% smectite layers is recorded, along with subordinate smectite having 13% chlorite layers. In contrast, smectite is dominant in CH7-10 from 435 m, but on the XRD pattern there is a superlattice peak at 31.6 Å, generally taken as indicative of corrensite whose peak positions equate with ~58% chlorite layers. This identification is not positive because there are no subsequent rational series of peaks developed to confirm the identification, and such superlattice peaks are absent from all but two other samples in the three boreholes. In sample CH7-15, from 550 m, the assemblage is dominated by chlorite that has ~13% smectite layers, and minor smectite and corrensite (Fig. 3, Table 2a). Where smectite is of minor abundance in these samples, it shows only the basal 001 peak (no additional higher order reflections are present).

In the samples from greater depth at 641, 1001, 1003, and 1404 m (CH7-17, CH7-20, CH7-22, and CH7-38), chlorite is the only mafic phyllosilicate and has chlorite layers in the range 94–97% (Fig. 3). Illitic minerals are less common and less abundant, comprising illite/smectite and illite in about half the samples (Table 2a). The change from smectite- to chlorite-dominant assemblages takes place at the level of rapidly rising temperatures over the depth interval of ~300–500 m (Fig. 3).

EMP data for phyllosilicates are available only from cored samples at 484 m and deeper. The analyses of mafic phyllosilicates from samples at 484 and 486 m recalculate to chlorite/smectite with chlorite layers of ~75%. Below 500 m, the analyses recalculate to chlorite/smectite with higher proportions of chlorite layers in the range 88–93%. These values contrast somewhat with the XRD determinations, which indicate fewer mixed-layers. This kind of discrepancy between XRD and EMP determinations is common (Schiffman and Fridleiffson 1991). The EMP-determined smectite contents are largely the result of variable Ca concentrations, which are ~0.40 wt% and 0.1–0.2 wt% in samples from less than and more than 500 m depth, respectively. All EMP analyses have a restricted compositional range, with formula proportions of Si = 5.5–6.2

TABLE 1b. EMP analyses of mafic phyllosilicates from cored samples from well CH8

sample	236 (9)	sd	941 (4)	sd	941 (7)	sd	962 (14)	sd	962 (21)	sd	1206 (16)	sd	1558 (6)	sd	2000 (6)	sd	2556.00	sd
SiO_2	45.96	5.33	27.65	1.33	27.72	1.19	27.45	1.21	28.07	1.64	25.64	1.31	27.33	1.07	28.50	0.27	24.48	0.31
TiO_2	0.23	0.41					0.03	0.04	0.03	0.03	0.03	0.05	0.04	0.07	0.00	0.00	0.03	0.03
Al_2O_3	11.83	2.96	18.14	0.89	18.55	1.01	18.15	0.39	18.59	0.86	18.50	0.44	19.88	0.78	16.81	0.38	17.38	0.53
FeO_T	7.99	2.11	26.99	0.99	26.55	1.09	25.90	0.85	25.08	1.66	23.17	0.77	15.37	0.94	22.14	0.49	30.06	0.44
MnO	0.48	0.13	0.38	0.03	0.37	0.05	0.36	0.05	0.35	0.07	0.65	0.10	0.58	0.05	0.63	0.04	0.76	0.07
MgO	10.10	3.71	12.96	0.89	12.49	0.91	12.72	0.94	12.36	1.07	14.58	1.01	20.36	1.01	17.48	0.58	10.29	0.27
CaO	1.61	0.57	0.50	0.11	0.61	0.26	0.24	0.06	0.23	0.06	0.16	0.03	0.15	0.07	0.32	0.06	0.14	0.15
Na_2O	0.51	0.59	0.15	0.04	0.17	0.07	0.07	0.02	0.07	0.02	0.23	0.06	0.16	0.02	0.10	0.03	0.22	0.04
K_2O	0.29	0.47	0.07	0.02	0.25	0.37	0.24	0.15	0.52	0.51	0.04	0.01	0.09	0.06	0.05	0.01	0.07	0.02
Total	79.00	5.17	86.83	1.34	86.71	1.44	85.15	2.22	85.30	2.04	82.99	2.82	83.94	3.26	86.03	0.76	83.43	1.12
Formulae based on 28 O atoms																		
Si	9.34	0.37	5.94	0.16	5.95	0.13	5.98	0.11	6.07	0.19	5.69	0.11	5.71	0.07	6.03	0.03	5.65	0.08
Ti	0.04	0.06	0.00	0.00	0.00	0.00	0.00	0.01	0.00	0.01	0.00	0.01	0.01	0.01	0.00	0.00	0.01	0.01
^{IV}Al	0.00	0.00	2.06	0.16	2.05	0.13	2.02	0.11	1.93	0.19	2.31	0.11	2.29	0.07	1.97	0.03	2.35	0.08
^{IV}Al	2.83	0.51	2.54	0.15	2.65	0.23	2.65	0.10	2.82	0.29	2.53	0.07	2.61	0.07	2.23	0.10	2.38	0.03
Fe	1.36	0.45	4.85	0.29	4.77	0.26	4.72	0.23	4.54	0.38	4.30	0.15	2.69	0.12	3.92	0.08	5.81	0.08
Mn	0.08	0.03	0.07	0.01	0.07	0.01	0.07	0.01	0.06	0.01	0.12	0.02	0.10	0.01	0.11	0.01	0.15	0.01
Mg	3.06	1.31	4.15	0.23	4.00	0.28	4.13	0.21	3.98	0.32	4.82	0.18	6.34	0.15	5.51	0.17	3.54	0.06
NIC	16.71	0.91	19.61	0.11	19.49	0.21	19.57	0.10	19.40	0.30	19.78	0.06	19.75	0.05	19.77	0.06	19.88	0.03
Ca	0.35	0.10	0.12	0.02	0.14	0.06	0.06	0.02	0.05	0.02	0.04	0.01	0.03	0.02	0.07	0.01	0.03	0.03
Na	0.20	0.22	0.06	0.02	0.07	0.03	0.03	0.01	0.03	0.01	0.10	0.02	0.06	0.01	0.04	0.01	0.10	0.02
K	0.08	0.12	0.02	0.01	0.07	0.10	0.07	0.04	0.14	0.13	0.01	0.00	0.02	0.02	0.01	0.00	0.02	0.01
IC	0.63	0.41	0.20	0.03	0.28	0.12	0.15	0.04	0.23	0.13	0.15	0.02	0.12	0.03	0.13	0.02	0.15	0.04
XMg	0.69	0.06	0.46	0.02	0.46	0.02	0.47	0.02	0.47	0.02	0.53	0.02	0.70	0.01	0.58	0.01	0.38	0.01
x	0.00	0.00	0.78	0.06	0.72	0.10	0.76	0.05	0.68	0.14	0.88	0.03	0.86	0.03	0.87	0.03	0.93	0.01
Formulae based on variable number of O atoms as indicated																		
Ox	22.0		26.7		26.3		26.6		26.1		27.3		27.2		27.2		27.6	
Si	7.34	0.23	5.88	0.16	5.89	0.13	5.92	0.11	6.01	0.19	5.63	0.11	5.65	0.06	5.97	0.03	5.59	0.08
^{IV}Al	0.66	0.23	2.12	0.16	2.11	0.13	2.08	0.11	1.99	0.19	2.37	0.11	2.35	0.06	2.03	0.03	2.41	0.08
Ti	0.03	0.05	0.00	0.00	0.00	0.00	0.00	0.01	0.00	0.01	0.00	0.01	0.01	0.01	0.00	0.00	0.00	0.01
^{VI}Al	1.57	0.60	2.42	0.14	2.54	0.23	2.54	0.10	2.70	0.29	2.42	0.07	2.50	0.07	2.12	0.10	2.27	0.03
Fe	1.07	0.37	4.80	0.28	4.72	0.26	4.67	0.23	4.49	0.38	4.26	0.15	2.66	0.12	3.88	0.08	5.74	0.08
Mn	0.06	0.02	0.07	0.01	0.07	0.01	0.07	0.01	0.06	0.01	0.12	0.02	0.10	0.01	0.11	0.01	0.15	0.01
Mg	2.40	1.07	4.11	0.22	3.95	0.28	4.09	0.20	3.94	0.32	4.77	0.17	6.28	0.14	5.45	0.16	3.50	0.06
NIC	13.13	0.82	19.40	0.11	19.28	0.20	19.37	0.10	19.20	0.30	19.58	0.05	19.54	0.05	19.56	0.06	19.67	0.03
Ca	0.28	0.08	0.11	0.02	0.14	0.06	0.06	0.02	0.05	0.02	0.04	0.01	0.03	0.02	0.07	0.01	0.03	0.03
Na	0.16	0.17	0.06	0.02	0.07	0.03	0.03	0.01	0.03	0.01	0.10	0.02	0.06	0.01	0.04	0.01	0.10	0.02
K	0.06	0.09	0.02	0.01	0.07	0.10	0.07	0.04	0.14	0.13	0.01	0.00	0.02	0.02	0.01	0.00	0.02	0.01
IC	0.49	0.32	0.19	0.03	0.28	0.12	0.15	0.04	0.23	0.13	0.15	0.02	0.12	0.03	0.13	0.02	0.15	0.04
T °C	44	38	280	26	278	21	273	17	258	31	319	18	316	10	265	5	326	12

Notes: Figure under sample heading is depth (m) of sample in well, and number of repeat analyses given in parentheses for which standard deviation (sd) is calculated. x value is percentage of chlorite layers, and *T* °C is temperature derived from chlorite thermometer. FeO_T total iron as FeO.

(cations per 28 O atoms) and values of Fe/(Fe+Mg) = 0.39–0.54, which are equivalent to pycnochlorite.

Well CH8. The phyllosilicate minerals from CH8 were examined in 12 XRD and six EMP samples, and show similar trends to those in CH7. Little core material is available at depths shallower than ~1000 m and the data are mostly from XRD, whereas at greater depths, both XRD and EMP data are available. Figure 4 and Table 2b show summaries of the XRD and EMP data in relation to depth and down-well temperatures. XRD patterns for three separated <2 μm clay fractions from samples over the range 236–700 m are shown in Figure 6.

For samples from depths shallower than ~500 m (CH8-2, CH8-6, and CH8-8; <120 °C), pure smectite or smectite with few (<15%) chlorite layers are the only mafic phyllosilicates recorded (Fig. 4). Strong basal reflections were recorded with weaker periodic reflections present to 005 (Fig. 6a). The XRD pattern of sample CH8-13 from 551 m (170 °C) shows a three-phase phyllosilicate assemblage of corrensite, smectite, and chlorite (Fig. 6b). A weak superlattice peak at 31.3 Å with accompanying 002 (15.4 Å) and 004 (7.6 Å) reflections represents the best XRD evidence in the three wells of corrensite whose peak positions are indicative of ~58% chlorite layers. There is an additional 16.5 Å peak interpreted as a basal smectite reflection but which has no further resolvable periodic reflections. The position of the basal reflection is indicative of some 18% chlorite layers. A further weak peak at 7.28 Å is interpreted as an 002 reflection from chlorite, although again there are no observable periodic reflections; this peak position is indicative of 80% chlorite layers.

From the next sampled depth at 700 m, to the base of the XRD sampled section at 1558 m, chlorite with few smectite mixed-layers (6–8%) is the only mafic phyllosilicate recorded by XRD (Figs. 4 and 6c), apart from one sample with 32% smectite layers. The change from smectite- to chlorite-dominated samples occurs at the step between the rapid rise in temperature and a more constant thermal zone below ~500 m. No

TABLE 1C. EMP analyses of mafic phyllosilicates from cored samples from well CH9

Sample	1005 (14)	sd	1266 (9)	sd	1752 (9)	sd
SiO_2	30.47	0.28	26.45	0.58	25.85	0.74
TiO_2	0.03	0.04	0.00	0.00	0.03	0.05
Al_2O_3	15.26	0.48	18.94	0.53	19.54	0.29
FeO_T	23.88	0.89	24.39	4.08	23.79	1.03
MnO	0.48	0.06	0.45	0.05	0.59	0.07
MgO	16.43	0.41	14.26	2.43	15.18	0.95
CaO	0.81	0.26	0.20	0.08	0.15	0.04
Na_2O	0.02	0.01	0.04	0.03	0.04	0.02
K_2O	0.02	0.02	0.04	0.04	0.01	0.01
Total	87.41	1.01	84.73	1.59	85.18	1.03
Formulae based on 28 O atoms						
Si	6.38	0.08	5.75	0.08	5.59	0.07
Ti	0.01	0.01	0.00	0.00	0.01	0.01
^{IV}Al	1.62	0.08	2.25	0.08	2.41	0.07
^{IV}Al	2.15	0.06	2.61	0.09	2.57	0.04
Fe	4.18	0.14	4.44	0.77	4.30	0.24
Mn	0.09	0.01	0.08	0.01	0.11	0.01
Mg	5.12	0.13	4.62	0.76	4.89	0.24
NIC	19.54	0.10	19.76	0.05	19.87	0.03
Ca	0.18		0.05	0.02	0.03	0.01
Na	0.01	0.01	0.02	0.01	0.02	0.01
K	0.01	0.00	0.01	0.01	0.00	0.00
IC	0.20	0.07	0.08	0.01	0.05	0.02
XMg	0.55	0.01	0.51	0.08	0.53	0.03
x	0.75	0.05	0.86	0.03	0.93	0.02
Formulae based on variable number of O atoms as indicated						
Ox	26.5		27.2		27.6	
Si	6.03	0.06	5.58	0.06	5.50	0.06
^{IV}Al	1.97	0.06	2.42	0.06	2.50	0.06
Ti	0.01		0.00	0.00	0.01	0.01
^{VI}Al	1.60	0.09	2.30	0.07	2.40	0.05
Fe	3.96	0.16	4.31	0.76	4.23	0.25
Mn	0.08	0.01	0.08	0.01	0.11	0.01
Mg	4.85	0.16	4.49	0.73	4.81	0.22
NIC	18.49	0.29	19.17	0.16	19.56	0.11
Ca	0.17	0.05	0.04	0.02	0.03	0.01
Na	0.01	0.01	0.02	0.01	0.02	0.01
K	0.01	0.00	0.01	0.01	0.00	0.00
IC	0.19	0.06	0.07	0.01	0.05	0.02
T °C	254	10	327	10	341	9

Notes: Figure under sample heading is depth (m) of sample in well, and number of repeat analyses given in parentheses for which standard deviation (sd) is calculated. x value is percentage of chlorite layers, and *T* °C is temperature derived from chlorite thermometer. FeO_T total iron as FeO.

illitic minerals are recorded at depths less than ~700 m. Below this depth, all but one sample have illitic phases present in varying amounts, with illite layers varying between 83–100%.

EMP data also show a marked contrast in phyllosilicate types between the shallower and deeper levels of CH8. In the one cored sample from shallower than 1000 m—sample CH8-6 from 236 m (106 °C)—the mafic phyllosilicate analyses have low non-interlayer cation (NIC per 28 O atoms) totals (16.7) and high interlayer cation totals (0.63, 1.6 wt% CaO, Table 1). These compositional data recalculate to an end-member smectite and are in accord with the XRD data, although the lower-than-ideal NIC total of 17.9 for a tri-smectite indicates some dioctahedral character for the smectite with its relatively high Al contents. As shown in Figure 7, the average composition of this smectite plots mid-way between those of tri- and di-smectite. The EMP data from samples over the range 941–2556 m are indicative of dominantly chloritic material having 72–93% chlorite layers. For two samples shallower than 1000 m, the chlorite layers comprise 72–75% and increase to 86–93% below that depth (Fig. 4, Table 2b). As in CH7, the EMP data typically indicate mixed-layering contents somewhat higher than those derived from XRD results (Fig. 4). All EMP analyses fall in a restricted compositional range, with formula proportions of Si = 5.7–6.1 (cations per 28 O atoms) and values of Fe/(Fe+Mg) = 0.30–0.54, which are equivalent to pycnochlorite.

TABLE 2a. XRD and EMPA results for <2 μm fractions from well CH7

Sample	Depth(m)/*T* (°C)	Sm	Co	Chl	Chl-EMPA	I/S
CH7-3	100/117	X-0				x-53
CH7-7	284/122	X-0		x-91		
CH7-8	350/127	x-13		X-87		x
CH7-10	435/140	X-13	x-55			
CH7-12	484/160				75	
CH7-13	486/160			X-91	74	x-80
CH7-15	550/180	x-7	x -58	X-87		
CH7-17	641/164			X-94	87	X-90
CH7-19	803/164				80	x
CH7-20	1001/164			X-94	83	X -90
CH7-22	1003/164			X-94	82	
CH7-28	1404/182			X-97	91	

Notes: X, major phase; x, minor phase. Figures under columns labeled as Sm, Co and Chl are XRD-determined percentage of chlorite layers. Those under Chl-EMPA are recalculated from probe data. Columns labeled as I/S are XRD-determined percentage illite layers.

TABLE 2b. XRD and EMPA results for <2 μm fractions from well CH8

Sample	Depth(m)/*T* (°C)	Sm	Co	Chl	Chl-EMPA	I/S
CH8-2	50/100	X- 0				
CH8-6	236/106	X- 4			0	
CH8-8	300/120	X-10				
CH8-13	551/170	X-8	x-58	x-80		
CH8-16	700/170			X-94		x-90
CH8-20	768/169			X-68		X-100
CH8-24a	801/168			X-92		X-95
CH8-26	941/178				75	x-90
CH8-29	950/177			X-94		X-83
CH8-30	962/176			X-94	72	X-88
CH8-33	1100/176			X-94		
CH8-36	1206/178			X-94	88	x-89
CH8-40	1558/182			X-94	86	
CH8-42a	2006/182				87	
CH8-49	2556/228				93	

Notes: X, major phase; x, minor phase. Figures under columns labeled as Sm, Co and Chl are XRD-determined percentage of chlorite layers. Those under Chl-EMPA are recalculated from probe data. Columns labeled as I/S are XRD-determined percentage illite layers.

TABLE 2c. XRD and EMPA results for <2 μm fractions from well CH9

Sample	Depth(m)/*T* (°C)	Sm	Chl	Chl-EMPA	I/S
CH9-1	50/98	X-0			
CH9-4	200/100	X-13			
CH9-6	300/144	X-4	x-93		x-46
CH9-10	504/175	X-6	x-98		
CH9-13	650/182	X-7	X-96		x-61
CH9-16	800/191	X-8	X-96		X-82
CH9-18	950/195	x-5	X-97		X-85
CH9-20	1005/196		X-94	75	
CH9-24	1150/184		X-93		x-85
CH9-29	1266/179		X-93	86	X-90
CH9-32	1752/214		X-93	93	x
CH9-35	2001/223		X-97		x-86

Notes: X, major phase; x, minor phase. Figures under columns labeled as Sm, Co and Chl are XRD-determined percentage of chlorite layers. Those under Chl-EMPA are recalculated from probe data. Columns labeled as I/S are XRD-determined percentage illite layers.

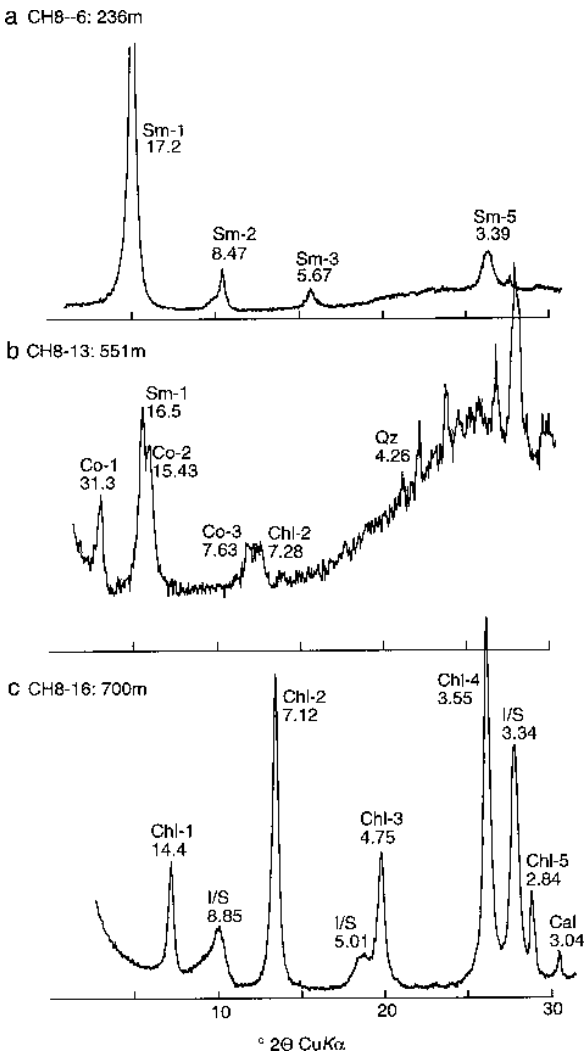

FIGURE 6. XRD patterns using Cu*K*α radiation for <2 μm fractions for samples from 236, 551, and 700 m depth in well CH8. (**a**) Monomineralic smectite sample with peaks labeled as Sm-1, Sm-2, etc. for first, second etc. periodic reflections. (**b**) Polymineralic sample with corrensite (Co), smectite (Sm), and chlorite (Chl), periodic peaks labeled as for a. (**c**) Sample with chlorite as only mafic phyllosilicate and illite/smectite (I/S), periodic peaks labeled as for a.

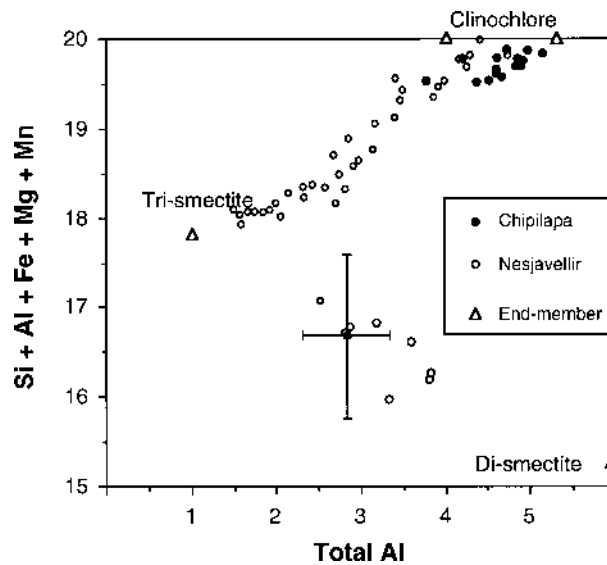

FIGURE 7. Electron microprobe chemical data (1σ error bars) for mafic phyllosilicates from Chipilapa and Nesjavellir geothermal systems. Non-interlayer cation (NIC; Si+Al+Fe+Mg+Mn) totals plotted against total Al content. All chemical data calculated on the basis of a chlorite formula with 28 O atoms. On this basis ideal tri-smectite plots with 17.92 NIC and clinochlore with 20 NIC. Data from sample CH8-6 plot in an intermediate position between the tri- and di-smectite end-members. All other Chipilapa data are for near pure end-member chlorite that plots close to clinochlore position. Nesjavellir data are from Schiffman and Fridleifsson (1991) and show a continuous chlorite/smectite mixed-layer series between the two end-members.

Well CH9. The distribution of mafic phyllosilicates in CH9 as determined from 12 XRD and three EMP samples is similar to CH7 and CH8, but the phase transitions occur at slightly greater depth and over a larger depth range and higher temperature (Fig. 5). Smectite with <15% chlorite layers (XRD) is the only mafic phyllosilicate phase in the two shallowest samples (CH9-1 and CH9-4) at 50 and 200 m. In the next five samples over the depth range 300–950 m, both smectite and chlorite are present, each being nearly pure minerals with <10% mixed layers (Fig. 5, Table 2c). Over this 650 m depth range, the gradual change from a smectite- to a chlorite-dominant assemblage is clearly shown in Figure 8; there is no corrensite recorded in any sample over this range. Each phase has a clear and distinctive periodic peak sequence from 001 to 005 for smectite and 001 to 003 for chlorite. In six samples from 950 m (195 °C) to the well base at 2001 m, the mafic phyllosilicate is only chlorite (Fig. 5).

Illitic minerals are again variably developed in terms of occurrence and abundance and show illite layers in the range 46–90% (Table 2c). A notable feature in the XRD pattern of sample CH9-6 from 300 m is the presence of a composite peak at 8.5–9.0 Å that is resolved into two peaks at 8.48 and 8.97 Å. These indicate mixed-layering with smectite progressing into both an illitic character (trioctahedral) and chloritic (dioctahedral) character.

Analyses from three samples at 1005, 1266, and 1752 recalculate to chlorite layers in the range 75–93% (Fig. 5, Table 2c). The three EMP analyses fall in a restricted compositional range, with formula proportions of Si = 5.6–6.4 cations (per 28 O atoms), and values of Fe/(Fe+Mg) = 0.45–0.49, which are equivalent to pycnochlorite except for the analysis from 1005 m, which is a diabanite.

INTERPRETATION AND DISCUSSION OF THE CONTROLS AND MINERALOGIC FEATURES OF THE SMECTITE-TO-CHLORITE TRANSITION

XRD and EMP analyses of the <2 μm mafic phyllosilicate fraction from the three wells CH7, CH8, and CH9 indicate that the smectite to chlorite transition predominates over a transition into illite. Mafic phyllosilicates were recorded in all samples, whereas the illitic series was recorded in about one-half of the samples examined. One of the most striking fea-

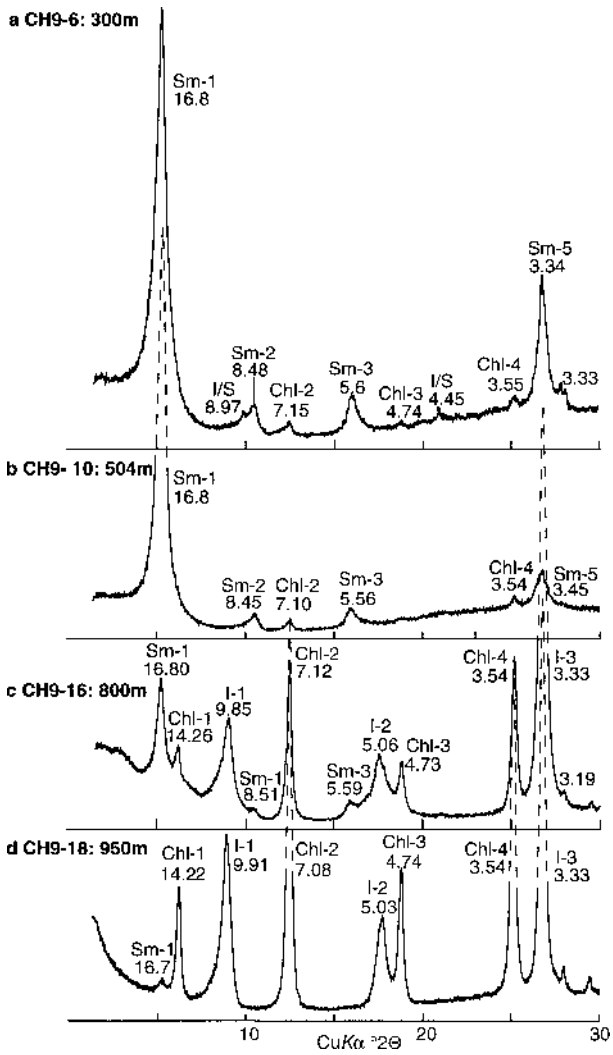

FIGURE 8. X-ray diffraction patterns using Cu*K*α radiation for <2 μm fractions for samples from 300, 504, 800, and 950 m depth in well CH9 that shows changing character of mafic phyllosilicates with depth. Peak labeling is as for Figure 6. **(a)** Sample with smectite and minor chlorite and illite/smectite. **(b)** As for **a**, but without illite/smectite. **(c)** Sample with same mineralogy as for **a**, but showing increasing amount of chlorite. **(d)** Sample with same mineralogy as for a, but showing dominance of chlorite and illite (I).

tures in the Chipilapa system is the clear dominance of the two end-members of the transition, smectite and chlorite, with XRD recording an extremely limited range of mixed layering. In smectite, mixed-layering with chlorite layers is below 20% in all cases, whereas for chlorite, it is <15% smectite layers except for one sample with 32%. The EMP data typically record higher amounts of mixed-layering, which is related largely to the contents of interlayer cations (Ca+Na+K). Greater credence is given to the XRD-determined results because small amounts of contamination or intergrowth with other phases can result in apparently high mixed-layer contents when recalculated from EMP data (Robinson et al. 1993). Recent TEM and AEM data on chlorite from low-grade rocks suggest that interlayer cations in excess of 0.05 per 28 O atoms are anomalous and due to contamination (Schmidt et al. 1999). The other notable feature is the restricted occurrence of corrensite, which is recorded in minor abundance in only three samples. These data are generally in accord with the results of Beaufort et al. (1995) and Patrier et al. (1996), who recorded virtually no mixed layers in smectite and typically <10% mixed layers in chlorite, although they recorded corrensite more commonly. In their <2 μm fractions, corrensite was present as a major phase in only ~8% of the samples examined, whereas in the <0.2 μm fractions from the two wells (CH7 and CH9) examined by Patrier et al. (1996), corrensite was present in a greater proportion of samples (~38%), and was a main phase in ~25%.

The dominance of the end-members, smectite and chlorite, is a striking feature of this geothermal system, compared to some others, and the reasons for this particular style is an important matter to consider in the present debate about the smectite to chlorite transformation. There are several factors, apart from temperature that have been proposed as controlling features of this transformation including whole-rock lithology and chemistry, as well as successive recrystallization events in geothermal systems, and these are now considered.

Whole-rock control

A lithologic control between smectite- and chlorite-dominated development in low-grade metabasite flows was documented by Schmidt and Robinson (1997). These authors showed that, on a within-flow scale of a few meters, smectite was restricted to massive flow centers but chlorite dominated in highly amygalodial flow tops. This was attributed to original permeability differences linked to fluid flow patterns having a control on phyllosilicate type. In the present study, such small scale differences in phyllosilicate types have not been observed; instead, in all three wells, there is a clear distinction between smectite and chlorite at shallower and deeper levels, respectively. This distinction occurs despite samples being from interbedded lower and higher permeability lava and pyroclastic horizons that have the same phyllosilicate type (Figs. 3, 4, and 5). These data suggest that lithology is not a controlling factor on the mafic phyllosilicate distribution in the Chipilapa system, a conclusion reached also by Patrier et al. (1966), who determined that lithology had no direct control on clay precipitation.

Most previous reports on the smectite to chlorite transition have been from basaltic systems. In the present calc-alkaline setting, the whole-rock chemistry is more siliceous and aluminous and may be a controlling influence on the character of mafic phyllosilicates. However, the calc-alkaline system of the Newberry Caldera, Oregon, which is also dominated by andesitic to dacitic compositions, displays the same continuous smectite through chlorite/smectite to chlorite transition (Keith and Bargar 1988) as seen in basaltic systems. Although the character of the smectite to chlorite transition is markedly different between Chipilapa and the basaltic Nesjavellir system in Iceland, the starting and ending compositions of the two series are closely similar. In both cases the smectite compositions are nearly identical, lying midway between the tri- and di-smectite end-members (Fig. 7) and have the same maximum

Al content of 3.8 cations (per 28 O atoms). In addition, both end-member chlorite compositions have similar contents of total Al (= 4.98 and 4.8/per 28 O atoms, respectively; Fig. 7). These comparisons suggest that the differences between the broadly basaltic and calk-alkaline settings are not the primary control on the characteristic style of mafic phyllosilicate development in Chipilapa. Also, the chlorite in the three Chipalapa wells has a restricted compositional range in terms of its Si contents and values of Fe/(Fe+Mg) (Table 2), which equate to pycnochlorite in all but one sample. A much broader range from ripidolite to diabanite was reported in basaltic dikes and sills from the Point Sal Ophiolite by Bettison and Schiffman (1988). Thus, any whole-rock chemical variation is not reflected in major changes in the chemistry of the Chipilapa phyllosilicates, a conclusion also reached by Paltrier et al. (1996).

Clay precipitation in different thermal regimes?

In any geothermal system, there is always some uncertainty about whether any observed mineral distributions or zonations reflect measured temperature profiles, or if they are related to some previous thermal events and regimes. In the case of Chipilapa, where the dominance of end-member smectite and chlorite contrasts with basaltic systems having a smectite-chlorite/smectite-chlorite transformation, there is an obvious concern that the two minerals might have crystallized in different events. The regular change with depth seen here in all wells from only smectite at shallower levels, to an intermediate-depth transition zone of smectite and chlorite with local corrensite, followed by a deeper zone of only chlorite, points to a transformation sequence rather than an overprinted association. The same conclusion was reached by Bril et al. (1996), who identified conversion series of illite/smectite and chlorite/saponite that were almost complete in the four Chipilapa wells they examined. However, other work by Patrier et al. (1996) revealed some lack of agreement between clay mineral distributions for the <0.2 μm fractions from the Chipilapa wells and that of the "classic patterns" of the smectite/illite and saponite/chlorite conversions. In particular, they recorded smectite throughout well CH7B (not studied here), with very extensive development at certain levels, and smectite together with corrensite and/or chlorite over the depth range from 306 m to the base at ~1150 m. In Well CH9, smectite was recorded to ~1200 m overlapping with chlorite from a depth of 400 m. However, in the coarser <2 μm fractions from the present study, smectite does not extend beyond a depth of 950 m in CH9 . The differences in the clay distribution between those recorded here and those of Patrier et al. (1996) can be accounted for by their use of different clay-size fractions and examination of wells from different locations, features that are considered further below.

Transition with respect to temperature

One of the obvious advantages of examining clay distributions in active geothermal systems is that some constraints on the temperature stability of these minerals might be obtained. As discussed above, in geothermal systems there is always the concern that measured well temperatures may not be those under which the observed mineralogy developed. However, as shown above, other factors such as whole-rock lithology and chemistry, or successive clay precipitation, do not appear to be major controlling variables in Chipilapa, suggesting the importance of temperature. Further evidence in support of this conclusion is provided by comparisons between mineral distributions (principally zeolites) in Chipilapa and other geothermal systems. The progressive downwell occurrence of heulandite, mesolite, stilbite, mordenite, analcime, laumontite, and wairakite, is a direct match to the sequence developed in Icelandic geothermal areas (Kristmannsdóttir and Tómasson 1978). The temperature range for this Chipilapa progression from 106 to 170 °C compares closely with an equivalent range of ~70 to 170 °C for Icelandic systems (Kristmannsdóttir and Tómasson 1978).

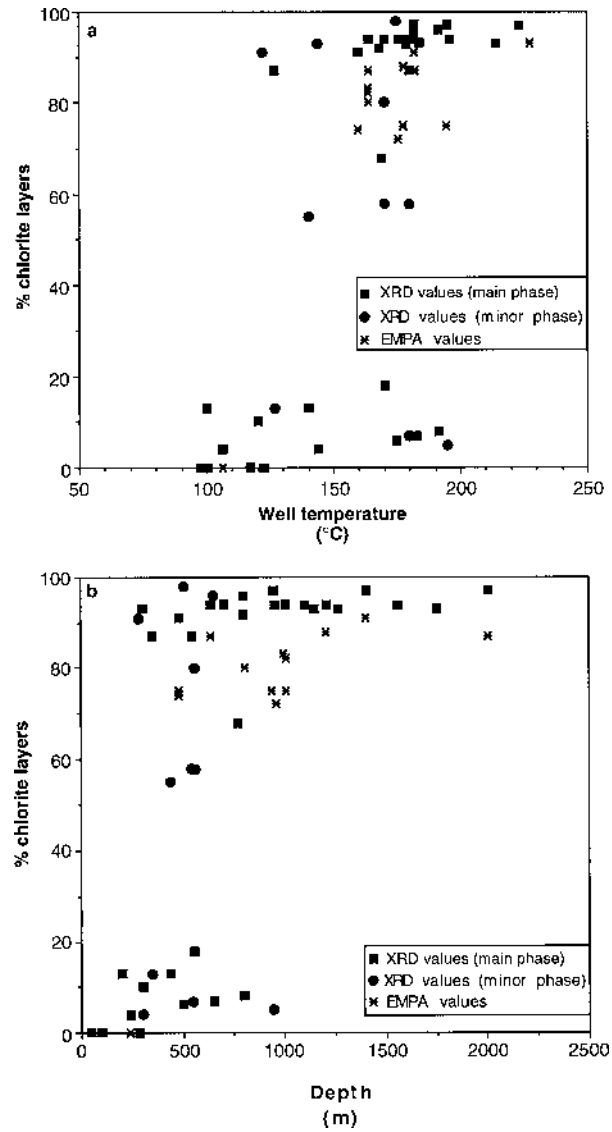

FIGURE 9. Diagram showing percentage chlorite layers as determined by XRD in mafic phyllosilicates in all three wells plotted against **(a)** well temperature and **(b)** well depth. The data shows the clear and sharp distinction between smectite with <20% chlorite layers and chlorite with less than ~10% smectite layers.

Variations in chlorite layers in the smectite, corrensite, and chlorite phases with respect to temperature and depth in the three wells are shown in Figure 9. In the present study, smectite was recorded up to a temperature of ~195 °C, and to a virtually identical temperature of ~200 °C for both the <2 μm and <0.2 μm fractions by Beaufort et al. (1995) and Patrier et al. (1996) respectively. Corrensite in the samples examined here is very restricted and limited in abundance, being recorded in only three samples; the occurrence of corrensite thus cannot be matched satisfactorily with depth or temperature. In the <2 μm fractions of Beaufort et al. (1995), corrensite was recorded over a temperature range from ~110–200 °C, but was present as a main phase in only ~8% of the samples over that temperature range. In the <0.2 μm fractions, corrensite was recorded over a similar temperature range of 120–185 °C (Patrier et al. 1996), and was a main phase in only ~30% of the samples over that temperature range. In the present study, chlorite is found in abundance from ~160 °C to the maximum recorded temperature of ~230 °C. Chlorite is recorded as low as ~120 °C, but is present in only three samples and it is of minor abundance in two (Fig. 9a). Comparison with the <0.2 μm and <2 μm data from Beaufort et al. (1995) and Patrier et al. (1996) shows a very close correspondence. They recorded chlorite in the <2 μm fractions as a minor phase from 110 °C, and as a major phase from 170 °C; in the <0.2 mm fractions, they recorded chlorite as a minor phase (from 132 °C), and as a major phase from 160 °C. In the present case there is an overlap between smectite and chlorite occurrences over a small vertical depth interval of ~500 m before abundant chlorite is recorded at deeper levels (Fig. 9b).

In their analysis of the <0.2 μm clay fraction from Chipilapa Wells, Patrier et al. (1996) considered the poor correlation between clay distribution and depth and temperature was not in accord with "classic patterns" of clay distribution. In particular they considered that smectite was present at temperatures much higher than in other natural systems. In the Nesjavellir geothermal field in Iceland, di- and tri-octahedral smectite is dominant below ~180 °C, followed by mixed-layer chlorite/smectite to 240 °C, then corrensite to 265 °C and above 270 °C, discrete chlorite appeared. Similar results were also recorded by Kristmannsdóttir (1979) in other Icelandic geothermal systems where smectite was recorded as transforming to chlorite at 150–200 °C, with chlorite becoming predominant from ~230 °C. Also in the Newberry caldera of the Cascade range, Keith and Bargar (1988) recorded smectite up to ~ 200 °C, with the first occurrence of chlorite/smectite and chlorite from ~150 °C. These comparisons suggest that the upper limit of smectite in the Chipilapa field at ~190 °C is entirely compatible with other geothermal occurrences. However, a marked contrast with other geothermal systems is the low temperature (~160 °C) at which chlorite becomes dominant instead of a transition zone of intermediate temperatures (~180–230/270 °C) that has abundant mixed-layer minerals and/or corrensite. Indeed, a notable feature of the data from wells CH7 and CH9 is the respective temperature ranges from 122–180 °C and 144–195 °C that mark the conversion from smectite to chlorite, which involve temperature spans of only 51 and 58 °C, respectively. Moreover, the progression seen in CH9 is one of a gradual decrease in smectite and increase in chlorite abundances over the depth range 300–950 m. We regard the conversion from one mineral species to another, over a temperature range of <60 °C, as in the case here, to be rapid, which contrasts with the extensive overlap between these mineralogical species as proposed by Patrier et al. (1996).

The position and depth range over which the transition occurs provides an important comparison among the three wells. In CH7 (Fig. 3) there is a rapid rise in temperature from 350–550 m, with a marked thermal anomaly at 185 °C attributed to fracture fluid flow in a reservoir zone (Patrier et al. 1996). The same rapid rise in temperature is observed in CH8 at a similar depth range of 250–500 m (Fig. 4). In these wells the transition from smectite to chlorite occurs at exactly the same depth range at which this rapid rise in temperature is developed. Indeed, it is at the position of the thermal anomaly in CH7 that chlorite becomes a dominant phase in the <2 μm fraction rather than the place where abundant high-temperature smectite is precipitated, in contrast with the <0.2 μm fraction linked to zones of fluid influx associated with this permeable horizon (Patrier et al. 1996). The site of well CH9 is away from the thermal anomaly intersected by wells CH7 and CH8, and the temperature gradient is of a lower, more uniform character between ~300 and 1000 m. In this well, the transition from smectite to chlorite reflects this lower gradient in that the depth interval of smectite and chlorite overlap is extended from ~200–300 m, as in CH7, to an interval of more than 700 m. The temperature interval for the transition is, however, virtually the same in the two wells at 58 and 51 °C, respectively.

We conclude that the <2 μm mafic phyllosilicate fraction shows a general concordance between the smectite to chlorite transition and the observed well temperatures. This overall conclusion is derived from the following points: (1) the consistency among the data from these three wells; (2) the narrow range in temperature and depth overlap between smectite and chlorite; and (3) the similarity between the temperature range of smectite occurrence in Chipilapa and the Icelandic and Newberry geothermal systems. Overall, there appears to have been a major thermal control on the initiation of the smectite to chlorite transition and on the mafic phyllosilicate distributions in the CH7, CH8, and CH9 wells of the Chipilapa geothermal system. This conclusion is not fully in accord with that of Patrier et al. (1996) who considered that other controls, such as permeability, had a greater influence in the crystallization of smectite in the <0.2 μm fractions at high temperatures (170–205 °C) within zones of high permeability. Accordingly, the overlap in temperature range between smectite and chlorite was attributed largely to high-temperature smectite precipitation, associated with present-day fluid circulation, onto a previous chlorite-dominant assemblage.

Patrier et al. (1996) chose to examine <0.2 μm fractions on the basis this material would represent the most reactive part of the system and that minerals inherited from an earlier assemblage would be minimized. As itemized above, there is a great similarity between not only the temperatures ranges of smectite and chlorite distribution but also their respective depth overlap, suggesting that there may well be a common control(s) on clay mineral distribution between the two contrasting size fractions.

Some of the discrepancy in the results and interpretations between the different clay fractions is that Patrier et al. (1996)

examined clay separates from wells CH7, CH7B, and CH9, as opposed to wells CH7, CH8, and CH9 used in this study. Patrier et al. (1996) indicated that the main area of late-stage smectite precipitation is associated with a thermal anomaly and that CH7B is located at the maximum extent of this anomaly, whereas CH7 is at the edge, and CH8 and CH9 are outside the anomaly and away from the region of late-stage, high-temperature smectite precipitation.

The relationship between well temperature and ^{IV}Al in chlorite from the Chipilapa system is shown in Figure 10. All but one data point correspond to chlorite for which XRD data indicate low amounts of smectite mixed-layers (<10%). In these samples there is a variation in ^{IV}Al from 2.0–2.5 cations per formula unit, with no apparent compositional trend over a temperature range of 160–230 °C. The relationship between ^{IV}Al in chlorite and temperature from the Los Azufres geothermal system in Mexico and applied as a geothermometer by Cathelineau (1988), is shown by the solid line. The Chipilapa data are offset from the Azufres data and uncorrelated, which casts doubt on the general applicability of this geothermometer as noted previously by Jiang et al. (1994) based on other criteria.

Mineralogic features

The minimal mixed layering in the samples reported here provides strong support for a model involving a discontinuous change from smectite to chlorite, rather than one involving continuous mixed-layering of chlorite/smectite between the two end-members. A discontinuous transition also was recorded in a hydrothermal system of basic-intermediate composition from the La Palma seamount of the Canary Islands (Schiffman and Staudigel 1995) and in low-grade Keweenawan metabasites from Minnesota (Schmidt and Robinson 1997). In the <2 μm fractions from those localities, end-member smectite and chlorite were dominant but, in contrast with the present examples, well-crystallized corrensite was abundant and occurred as the sole mafic phyllosilicate in some samples. However, those reports contrast with data from a mafic geothermal system in Iceland where a continuous sequence of chlorite/smectite was recorded between the two end-members as shown in Figure 7 (Schiffman and Fridleiffson 1991). A possible explanation for these differences in the transition is that the discontinuous change is representative of an equilibrium prograde sequence, whereas the continuous change represents metastable crystallization in response to incomplete reaction or low integrated fluid/rock ratios (Schiffman 1995).

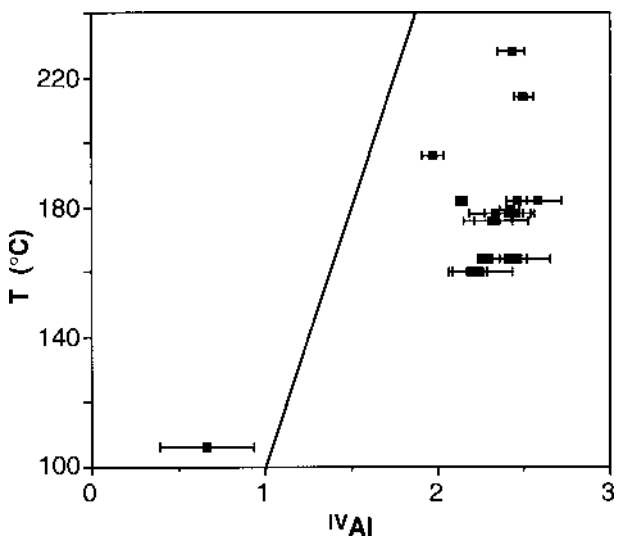

FIGURE 10. Plot of well temperature vs. ^{IV}Al content of mafic phyllosilicates. The Al content is calculated on the basis of variable number of O atoms related to percentage chlorite layers (x), ranging from 22 for a pure smectite to 28 for a clinochlore (Table 1). Straight line shows the relationship derived for the correlation between well temperature and tetrahedral Al content in chlorite from the Azufres geothermal system in Mexico (Cathelineau 1988).

In the Chipilapa geothermal system, there has been pervasive, secondary recrystallization (Santana de Zamora 1991). In addition there are extensive areas of high permeability (Patrier et al. 1996) so that there is a greater likelihood for high fluid/rock ratios. This is supported by data from the immediately adjacent Ahuachafan field, where over 1000 samples were examined from 31 wells drilled within a 6 km^2 area. Studies of the secondary mineralogy in those wells by Aumento et al. (1982) showed that pervasive geothermal alteration had proceeded with up to 90% recrystallization, of which clay mineral abundances reached 30% (plus additional chlorite); such extensive recrystallization implies very high fluid-rock ratios. Thus, in the Chipilapa system, the absence of a continuous chlorite/smectite mixed-layering sequence can be equated with a model of high fluid/rock ratios promoting an equilibrium transition, rather than a metastable chlorite/smectite transition.

Another feature that makes the Chipilapa system distinctive in the samples analyzed here is the rarity of corrensite and, where present, its diminutive superlattice peak in the <2 μm (Fig. 6) or the <0.2 μm (Fig. 3 of Patrier et al. 1996) fractions compared to its abundance and well-developed periodic diffraction sequences reported in other examples (Fig. 4 of Schiffman and Staudigel 1995; Fig. 9 of Schmidt and Robinson 1997). One possibility might relate to kinetic effects in geothermal systems where thermal gradients are high compared to regional settings. However, the thermal gradient of ~50 °C/km recorded in the Chipilapa wells is not high for a geothermal setting and is substantially lower than the >100 °C/km reported from the Nesjavellir, Icelandic field (Schiffman and Fridleiffson 1991). Therefore, kinetics in response to varying thermal gradients does not provide a satisfactory explanation for the differences in clay mineralogy.

The progression from smectite to chlorite observed here in the <2 μm fraction from the Chipilapa geothermal system is the most discontinuous step recorded. To date the reported data on this series have involved evidence of either (1) a more continuous chlorite/smectite mixed-layering (Liou et al. 1985; Bettison-Varga et al. 1991; Schiffman and Fridleiffson 1991; Robinson et al. 1993) or (2) discontinuous steps of smectite-corrensite-chlorite, with corrensite as a commonly occurring phase (Hoshi 1988; Tribble 1991; Shau and Peacor 1992; Schmidt and Robinson 1997). Such marked differences in the evolution of the same mineralogic series raises doubts as to whether the series represents an equilibrium reaction sequence.

Further arguments and discussion on these points that utilize data from several different examples of the smectite to chlorite transition are given in Robinson et al. (unpublished data).

ACKNOWLEDGMENTS

Financial support from the British Council that allowed A.S.-Z. to spend a period in Bristol is gratefully acknowledged. S.H. Schmidt is thanked for comments on an earlier version of the manuscript, P. Schiffman and an anonymous reviewer for their constructive review comments, and R.F. Dymek for editorial assistance.

REFERENCES CITED

Aumento, F., Viale, P., Choussy, M., and Santan, A. (1982) Alteration mineralogy of the Ahuachapan geothermal field. Geothermal Resources Council Transactions, 6, 7–10.

Beaufort, D., Papapanagiotou, P., Patrier, P., and Traineau, H. (1995) Les interstratifiés I-S et C-S dans les champs géothermiques actifs: sont-ils comparables a ceux des séries diagénétiques? Bulletin Centres Rech. Exploration-Production Elf Aquitaine, 19, 267–291.

Bettison, L.A. and Schiffman, P. (1988) Compositional and structural variations of phyllosilicates from the Point Sal ophiolite, California. American Mineralogist, 73, 62–76.

Bettison-Varga, L.A., Mackinnon, D.R., and Schiffman, P. (1991) Integrated TEM, XRD and electron microprobe investigation of mixed-layered chlorite/smectite from the Point Sal Ophiolite, California. Journal of Metamorphic Geology, 9, 697–710.

Bevins, R.E., Robinson, D., and Rowbotham, G. (1991) Compositional variations in mafic phyllosilicates from regional low grade metabasites and application of the chlorite geothermometer. Journal of Metamorphic Geology, 9, 711–721.

Bril, H., Papapanagiotou, P., Patrier, P., Lenain, J.F., and Beaufort, D. (1996) Fluid-rock interaction in the geothermal field of Chipilapa (El Salvador): contribution of fluid-inclusion data. European Journal of Mineralogy, 8, 515–531.

Cathelineau, M. (1988) Cation site occupancy in chlorites and illite as a function of temperature. Clay Minerals, 23, 471–485.

Cuellar, G., Choussy, M., and Escobar, D. (1981) Extraction-reinjection at Ahuachapan Geothermal Field, El Salvador. In L. Rybach and L.J.P. Muffler, Eds., Geothermal Systems: Principles and Case Histories, p. 321–336. Wiley, New York.

Essene, E.J. and Peacor, D.R. (1995) Clay mineral thermometry—a critical perspective. Clays and Clay Minerals, 43, 540–553.

Hoshi, K. (1988) Miocene ocean floor metamorphism during back-arc spreading in the Japan Sea. M.S. thesis, Stanford University, California.

Jiang, W-T. Peacor, D.R., and Buseck, P.R. (1994) Chlorite geothermometry?—contamination and apparent octahedral vacancies. Clays and Clay Minerals, 42, 593–605.

Keith, T.E.C. and Bargar, K.E. (1988) Petrology and Hydrothermal Mineralogy of U.S. Geological Survey Newberry 2 Drill Core from Newberry Caldera, Oregon. Journal of Geophysical Research, 93, 10,174–10,190.

Kristmannsdóttir, H. (1979) Alteration of basaltic rocks by hydrothermal activity at 100–300 °C. In M.M. Mortland and V.C. Farmer, Eds., Proceedings of the 6th International Clay Conference, p. 359–367. Elsevier, Amsterdam.

Kristmannsdóttir, H. and Tómasson, J. (1978) Zeolite zones in geothermal areas in Iceland. In L.B. Sand and F.M. Mumpton, Eds., Natural Zeolite Occurrence, Properties and Use, p. 277–284. Pergamon Press, Oxford.

Liou, J.G., Seki, Y., Guillemette, R.N., and Sakai, H. (1985) Compositions and parageneses of secondary minerals in the Onikobe geothermal system, Japan. Chemical Geology, 49, 1–20.

Patrier, P., Papapanagiotu, P., Beaufort, D., Traineau, H., Bril, H., and Rojas, J. (1996) Role of permeability versus temperature in the distribution of the fine (<0.2 μm) clay fraction in the Chipilapa geothermal system (El Salvador, Central America). Journal of Volcanology and Geothermal research, 72, 101–120.

Reynolds, R.C. (1980) Interstratified clay minerals. In G.W. Brindley and G. Brown, Eds., Crystal structures of the Clay Minerals and their X-ray identification, p. 249–303. Mineralogical Society, London, U.K.

—— (1988) Mixed-layer chlorite minerals. In Mineralogical Society of America Reviews in Mineralogy, 19, 601–629.

Robinson, D. and Bevins, R.E. (1994) Mafic phyllosilicates in low-grade metabasites—characterization using deconvolution analysis. Clay Minerals, 29, 223–237.

Robinson, D., Bevins, R.E., and Rowbotham, G. (1993) The characterization of mafic phyllosilicates in low grade metabasalts from eastern North Greenland. American Mineralogist, 78, 377–390.

Santana de Zamora, A. (1991) Mineralogia secundaria de los pozos CH-7 y CH-8 Campo Geothermico Chipolapa, El Salvador. Unpublished report Comision Ejecutiva Hidroelectrica Del Rio Lempa, San Salvador, El Salvador, 8 p.

Schiffman, P. (1995) Low grade metamorphism of mafic rocks. Review of Geophysics, Supplement, p. 81–86.

Schiffman, P. and Fridleifsson, G.O. (1991) The smectite to chlorite transition in drillhole NJ-15, Nesjavellir Geothermal Field, Iceland: XRD, BSE and electron microprobe investigations. Journal of Metamorphic Geology, 9, 679–696.

Schiffman, P. and Staudigel, H. (1995) The smectite to chlorite transition in a fossil seamount hydrothermal system: the basement complex of La Palma, Canary Islands. Journal of Metamorphic Geology, 13, 487–498.

Schmidt, D., Livi, K.J.T., and Frey, M. (1999) Investigation of chlorite, smectite and berthierine: an electron microbeam study of the Taveyanne greywacke, Switzerland. Journal of Metamorphic Geology.

Schmidt, S.T. and Robinson, D. (1997) Metamorphic grade and porosity/permeability controls on mafic phyllosilicate distributions in a regional zeolite to greenschist facies transition of the North shore Volcanic Group, Minnesota. Geological Society of America Bulletin, 109, 683–697.

Shau, Y.-H. and Peacor, D.R. (1992) Phyllosilicates in hydrothermally altered basalts from DSDP Hole 504B, Leg 83—a TEM and AEM study. Contributions to Mineralogy and Petrology, 112, 119–133.

Shau, Y.-H., Peacor, D.R., and Essene, E.J. (1990) Corrensite and mixed-layer chlorite/corrensite in metabasalt from northern Taiwan: TEM/AEM, EMPA, XRD and optical studies. Contributions to Mineralogy and Petrology, 105, 123–142.

Tribble, J.S. (1991) Clay mineral and zeolite diagenesis in the Toa-Baja well, Puerto Rico. Geophysical Research Letters, 18, 529–532.

MANUSCRIPT RECEIVED NOVEMBER 12, 1997
MANUSCRIPT ACCEPTED NOVEMBER 6, 1998
PAPER HANDLED BY PETER I. NABELEK